SAND2017-1388J

K-ε Turbulence Model Parameter Estimates Using an Approximate Self-Similar Jet-in-Crossflow Solution

Lawrence DeChant[1], Jaideep Ray[2], Sophia Lefantzi[2], Julia Ling[3], Srinivasan Arunajatesan[4]
Sandia National Laboratories, Albuquerque, NM and Sandia National Laboratories, Livermore, CA.

The k-ε turbulence model has been described as perhaps "the most widely used complete turbulence model." This family of heuristic Reynolds Averaged Navier-Stokes (RANS) turbulence closures is supported by a suite of model parameters that have been estimated by demanding the satisfaction of well-established canonical flows such as homogeneous shear flow, log-law behavior, etc. While this procedure does yield a set of so-called nominal parameters, it is abundantly clear that they do not provide a universally satisfactory turbulence model that is capable of simulating complex flows. Recent work on the Bayesian calibration of the k-ε model using jet-in-crossflow wind tunnel data has yielded parameter estimates that are far more predictive than nominal parameter values. Here we develop a self-similar asymptotic solution for axisymmetric jet-in-crossflow interactions and derive analytical estimates of the parameters that were inferred using Bayesian calibration. The self-similar method utilizes a near field approach to estimate the turbulence model parameters while retaining the classical far-field scaling to model flow field quantities. Our parameter values are seen to be far more predictive than the nominal values, as checked using RANS simulations and experimental measurements. They are also closer to the Bayesian estimates than the nominal parameters. A traditional simplified jet trajectory model is explicitly related to the turbulence model parameters and is shown to yield good agreement with measurement when utilizing the analytical derived turbulence model coefficients. The close agreement between the turbulence model coefficients obtained via Bayesian calibration and the analytically estimated coefficients derived in this paper is consistent with the contention that the Bayesian calibration approach is firmly rooted in the underlying physical description.

Nomenclature

c	=	constant
A	=	turbulent velocity scale constant
B	=	turbulent length scale constant
C	=	turbulent kinetic energy constant
C_μ	=	turbulence model constant
$C_{\varepsilon 1}$	=	turbulence model constant
$C_{\varepsilon 2}$	=	turbulence model constant
d	=	jet nozzle diameter (m)
D	=	turbulent dissipation constant
f	=	self-similar velocity function
g	=	self-similar turbulent kinetic energy function
h	=	self-similar turbulent dissipation function
J	=	jet momentum ratio
l	=	turbulent length scale (m)
L	=	distance separating counter-rotating vortices (m)
k	=	turbulent kinetic energy $(m/s)^2$
M	=	freestream Mach Number
n	=	self-similarity exponent
p'	=	impulse/length (kg/s)

[1] Technical Staff, Aerosciences Dept., P.O. Box 0825, Albuquerque, NM, 87185, Member AIAA.
[2] Technical Staff, Extreme-scale Data Science & Analytics, P.O. Box 969, Livermore, CA, 94551, Member AIAA.
[3] Truman Fellow, Thermal Fluid Science and Engineering, P.O. Box 969, Livermore, CA, 94551.
[4] Technical Management, Aerosciences Dept., P.O. Box 0825, Albuquerque, NM, 87185, Member AIAA.

P = turbulent production (m^2/s^3)
Re_T = turbulent Reynolds number
t = time (s)
u = streamwise velocity (m/s)
U = freestream velocity (m/s)
v = cross-stream velocity (m/s)
V_j = jet velocity (m/s)
W = normal velocity (m/s)
x = streamwise location (m)
y = cross-stream location (m)
z = normal distance (m)
α = locally defined constant
ε = turbulent dissipation (m^2/s^3)
ξ = y/l
Γ = circulation (m^2/s)
ρ = density (kg/m^3)
σ_k = turbulent kinetic transport coefficient
σ_ε = turbulent dissipation transport coefficient
τ = shear (Pa)

Subscripts/superscripts

j = jet
s = midstream value
* = dimensionless
0 = constant value
∞ = freestream, far-field

I. Introduction

Reynolds-Averaged Navier-Stokes (RANS) based simulations tend to be the "workhorse" for industrial fluid flow problems due to their ease-of-use and low computational overhead. A common closure hypothesis is the k-ε turbulence model which has been described by Pope[1] as perhaps "the most widely used complete turbulence model." Here "complete" signifies a turbulence model that provides closure to the Reynolds stresses without requiring additional information. The model relies upon a simple Boussinesq assumption[1,6,7] (effective turbulent viscosity analogy to molecular viscosity). It uses a scalar eddy viscosity approximation implying that a useful effective turbulent viscosity closure follows by identifying a turbulent velocity and length scale. The necessary length and velocity scales then results from solution of the kinetic turbulent energy equation and the turbulent dissipation. This type of modeling approach is by definition approximate and must be supported by a suite of model parameter constants[8]. Traditionally, the parameters have been estimated by solving the system of equations for simplified "unit-level" flow problems where well-known analytical or experimental data is available. Typical problems that are utilized include: homogeneous shear, law-of-the-wall and decaying homogeneous isotropic turbulence[1,8,9]. While requiring the model to honor the basic flows with the intent of identifying a "universal" set of turbulence parameters is laudable, the reality is less satisfactory. The values for the model parameters obtained using the traditional procedure (here referred to as the nominal set) tend to provide "plausible trend" solutions for many flows (especially simple ones) but are less suitable for complex flows. The variability associated with the specification of turbulence model constants, k-ε in particular, is well summarized by Pope[1].

As an alternative to using simplified flows to compute the turbulence model parameters, efforts to estimate their value by examining flows that are more closely aligned with the problem class of interest have also been developed. The approaches can range from case specific[10] (sometimes ad hoc) parameter adjustment to more sophisticated parameter estimations schemes[13]. A procedure based on Bayesian parameter estimation, developed by Ray et. al.[2,3,4,5], has demonstrated significant improvement in predictive ability for a class of jet-in-crossflow problems.

This process requires significant input from high quality simulation and/or experimental measurement. While perhaps daunting, the result is a predictive simulation capability for a practical but complex flow problem.

In this paper, however, we ask the question: can a simpler analytical solution that is more representative of the problem of interest be used to successfully estimate turbulence model parameters? Consequently, we seek a bridge between estimates drawn from simple canonical flows and coefficient values estimated from flows that are more closely aligned with a particular problem. Our approach is to derive and approximately solve a self-similar model for axisymmetric wake/jet flow. Though highly simplified, this solution will yield rigid constraints on the k-ε turbulence model constants: $\{C_\mu, C_{\varepsilon 1}, C_{\varepsilon 1}\}$ (we ignore the TKE and ε transport coefficients and define $\sigma_k = 1 \;\; ; \;\; \sigma_k = 1$) that are in general agreement with a more complex parameter estimation scheme. While analytical approaches are unlikely to be viable for highly complex flows, they nonetheless provide support for model calibration efforts by demonstrating connection between classical and recent procedures.

II. Governing Equations

Following the classical modeling approach for free-shear flows described by Tennekes and Lumley[6] we examine simplified Reynolds averaged expressions for momentum, turbulent kinetic energy (TKE) and turbulent dissipation[8] expressed in terms the streamwise velocity u, TKE *k* and turbulent dissipation ε. Assuming that the flow can be described by a self-similar approach we express the streamwise velocity as:

$$\frac{u}{u_s} = f(\frac{y}{l}) = f(\xi) \rightarrow u = u_s(x) f(\xi) \tag{1}$$

Here $u_s = u_s(x)$ is the maximum jet velocity defect, i.e. the centerline velocity "l" is the local turbulence length scale that changes with "x". The turbulent kinetic energy and dissipation follow as:

$$\begin{aligned} k &= k_s(x) g(\xi) \\ \varepsilon &= \varepsilon_s(x) h(\xi) \end{aligned} \tag{2}$$

We can relate velocity scale and the length scale to k and ε via the algebraic definitions: $k_s(x) = C u_s^2$ and $\varepsilon_s(x) = D\frac{u_s^3}{l}$. The partially linearized[6] governing equations associated with the flow of interest are the simplified axisymmetric momentum equation:

$$U\frac{\partial u}{\partial x} = \frac{1}{y}\frac{\partial}{\partial y}(y C_\mu \frac{k^2}{\varepsilon}\frac{\partial u}{\partial y}) \tag{3}$$

the turbulent kinetic energy:

$$U\frac{\partial k}{\partial x} = \frac{1}{y}\frac{\partial}{\partial y}(y C_\mu \sigma_k \frac{k^2}{\varepsilon}\frac{\partial k}{\partial y}) + C_\mu \frac{k^2}{\varepsilon}\left(\frac{\partial u}{\partial y}\right)^2 - \varepsilon \tag{4}$$

and turbulent dissipation

$$U\frac{\partial \varepsilon}{\partial x}=\frac{1}{y}\frac{\partial}{\partial y}(yC_{\mu}\sigma_{\varepsilon}\frac{k^2}{\varepsilon}\frac{\partial \varepsilon}{\partial y})+C_{\varepsilon 1}C_{\mu}k\left(\frac{\partial u}{\partial y}\right)^2-C_{\varepsilon 2}\frac{\varepsilon^2}{k} \tag{5}$$

where the effective viscosity is given by: $C_{\mu}\frac{k^2}{\varepsilon}$. The governing equations as represented by equations (3) - (5) are incompressible. While the class of problems that we will examine using results from this development have compressible features, we believe that the self-similar turbulent behavior that is the focus of our development is largely Mach number independent. Hence the incompressible approach is likely adequate. This conclusion was supported by an early analytical development where a compressibility correction term based upon a Sarkar-Zeman[11,12] dilatation-dissipation model was included in the TKE equation. Application of turbulence model parameters derived with the compressibility included to problems of interest showed uniformly worse agreement with measurements as compared to incompressible results suggesting that our incompressible modeling assumption is likely to be appropriate.

A. Self-Similarity

Following Tennekes and Lumley[6] our goal is to compute $u_s(x)$, $k_s(x)$, $\varepsilon_s(x)$ and $l(x)$ such that the governing equations will be invariant with "x", i.e. self-similar (self-preserving). We start with the momentum equation: $U\frac{\partial u}{\partial x}=\frac{1}{y}\frac{\partial}{\partial y}(y\frac{k^2}{\varepsilon}\frac{\partial u}{\partial y})$ and compute the term:

$$\frac{\partial u}{\partial x}=\frac{du_s}{dx}f-\frac{u_s}{l}\frac{dl}{dx}\xi\frac{df}{d\xi} \tag{6}$$

Putting these expressions back into the momentum equation gives:

$$U\left(\frac{du_s}{dx}f-\frac{u_s}{l}\frac{dl}{dx}\xi\frac{df}{d\xi}\right)=C_{\mu}\frac{u_s^2}{l}\frac{1}{y}\frac{d}{d\xi}\left(y\frac{k_s^2}{\varepsilon_s}\frac{g^2}{h}\frac{df}{d\xi}\right)=C_{\mu}\left(\frac{C^2}{D}\right)\frac{u_s^2}{l}\frac{1}{\xi}\frac{d}{d\xi}\left(\xi\frac{g^2}{h}\frac{df}{d\xi}\right) \tag{7}$$

(dividing through by $\frac{u_s^2}{l}$) and demanding self-similarity will require that the terms in $\frac{\frac{du_s}{dx}f-\frac{u_s}{l}\frac{dl}{dx}\xi\frac{df}{d\xi}}{\frac{u_s^2}{l}}$ be constant, which implies that

$$\frac{l}{u_s^2}\frac{du_s}{dx}=const$$

$$\frac{1}{u_s}\frac{dl}{dx}=const \tag{8}$$

These two expressions are a set of differential equations that will tell us the behavior of the length scale "l" and the velocity scale u_s. Additionally, via the algebraic definitions $k_s(x)=Cu_s^2$ and $\varepsilon_s(x)=D\frac{u_s^3}{l}$, the scaling behavior for k_s and ε_s will be available. We find that these expressions have a general solution[6] as

$$u_s = Ax^{n-1}$$

$$l = Bx^n \tag{9}$$

We still do not have an expression for "n" and require another equation.

Following the traditional analysis for axisymmetric wakes[1,6] we would propose that the jet momentum at any plane normal to the jet core flow direction is equal to the jet momentum at the nozzle exit[14] which is $\rho_j V_j^2 d^2 = \dot{m} V_j$. Here V_j is the velocity of the jet, ρ_j is the density of the jet and d the jet diameter. $\dot{m}$ is the jet's mass flow rate. We can therefore write

$$\frac{\pi}{4}\rho_j V_j^2 d^2 = const = 2\pi\rho_\infty \int_0^\infty Uuydy$$

$$= 2\pi\rho_\infty U u_s l^2 \int_0^\infty f\xi d\xi \tag{10}$$

Here ρ_∞ is the density of the freestream and U, its velocity. Equation (14) demands that $u_s l^2 = const \rightarrow n - 1 + 2n = 0 \rightarrow n = 1/3$. Given this formulation we can write

$$u_s = A^* U d^{2/3} x^{-2/3}$$

$$l = B^* d^{2/3} x^{1/3} \tag{11}$$

We emphasize that the preceding argument was based upon the approximation that the momentum constraint could be best described by $\rho_\infty Uu$, a plausible assumption for a wake/jet flow field or the transverse jet far from the jet exit[12]. Near the jet exit, however, the flow is clearly less influenced by the freestream velocity and the momentum constraint would be better modeled via $\rho_\infty uu$. Under this assumption, we formulate the constraint as $u_s^2 l^2 = const \rightarrow 2(n-1) + 2n = 0 \rightarrow n = 1/2$, implying that $u_s = A^* U d^{1/2} x^{-1/2} \quad ; \quad l = B^* d^{1/2} x^{1/2}$. This result is, of course, consistent with the 2-d wake/jet flow field[5] but is also valid for transverse jet near field behavior. The existence of two length and velocity scales describing near and far-field behavior of jet-in-crossflow has been described by several researchers[15] though clearly the far-field behavior dominates the jet trajectory behavior and is almost always described by the decay rates associated with equation (11)[16,17].

Thus, we are posed with a modeling challenge whereby we would like to retain both modeling similarity behaviors but would appear to be limited to one approach or the other. Indeed, consistency for self-similarity would appear to make any combination of these two behaviors incompatible. Here we focus on turbulence model parameter estimates. It will permit us to utilize a combination of the two similarity closures with one approach applied for flow field results and the other used to estimate turbulence model coefficients. We propose that

1. The momentum equation honors the far-field solution $u_s = A^* U d^{2/3} x^{-2/3} \quad ; \quad l = B^* d^{2/3} x^{1/3}$ thereby describing the streamwise varying behavior associated with jet-in-crossflow flowfield. This analysis is capable of modeling the flow field and turbulence quantities *given specified turbulence model parameters*. We compute the turbulence model coefficients utilizing the procedure described below.
2. The turbulence quantities k and ε are to be modeled using the near-field behavior - $u_s = A^* U d^{1/2} x^{-1/2} \quad ; \quad l = B^* d^{1/2} x^{1/2}$ - and solved to provided estimates for the turbulence model

parameters $\{C_\mu, C_{\varepsilon 1}, C_{\varepsilon 1}\}$. While the turbulence-based model parameters are necessarily based upon these near field expressions, we assign the turbulence Reynolds number to be consistent with the far-field value, i.e. $\mathrm{Re}_T = 14.1$ *We emphasize that the near-field approximation is only suitable to provide estimates for the turbulence constants, here* $\{C_\mu, C_{\varepsilon 1}, C_{\varepsilon 1}\}$ *while the far-field model is appropriate to provide mean, turbulent and trajectory information.*

B. Classical Turbulence Length and Velocity Scales (Far-field)

Following this prescription, we assume that $u_s = A^* U d^{2/3} x^{-2/3}$; $l = B^* d^{2/3} x^{1/3}$ (far-field) whereby the turbulent kinetic energy and dissipation follow from the definitions as: $k_s = CA^{*2} U^2 d^{4/3} x^{-4/3}$ and $\varepsilon_s = D \frac{A^{*3}}{B^*} \frac{U^3}{d} d^{7/3} x^{-7/3}$. Equation (7) then becomes

$$-\frac{B^*}{3A^*}\left(2f + \xi \frac{df}{d\xi}\right) = C_\mu \frac{C^2}{D} \frac{1}{\xi} \frac{d}{d\xi}\left(\frac{g^2}{h} \xi \frac{df}{d\xi}\right), \tag{12}$$

or, collecting terms

$$-\alpha\left(2f + \xi \frac{df}{d\xi}\right) = \frac{1}{\xi} \frac{d}{d\xi}\left(\frac{g^2}{h} \xi \frac{df}{d\xi}\right), \tag{13}$$

where we define $\alpha = \frac{B^*}{3A^*}\left(\frac{D}{C_\mu C^2}\right) = \frac{B^*}{3A^*}\mathrm{Re}_T$.

If we follow the classical approach utilized for wake/jet problems[1,6] we assume we approximate $\frac{g^2}{h} \approx const \approx 1$ and $\frac{D}{C_\mu C^2} = \mathrm{Re}_T = const$, where Re_T is approximately 14.1[6]. By defining $\alpha = 1$ we can solve the velocity function as $f = \exp(-\frac{1}{2}\xi^2)$, whereby the approximate momentum constraint gives $\frac{\pi}{4}\frac{\rho_j}{\rho_\infty}\frac{V_j^2}{U^2} = \frac{\pi}{4} J = A^* B^{*2} 2\pi \rightarrow A^* B^{*2} = \frac{J}{8}$. Here J represents the dimensionless jet momentum parameter[14,15,16], $J \equiv \frac{\rho_j}{\rho_\infty}\frac{V_j^2}{U^2}$. We can then solve the two expressions

$$\frac{B^*}{3A^*}\mathrm{Re}_T = 1 \quad ; \quad A^* B^{*2} = \frac{J}{8} \tag{14}$$

to give

$$A^* = \frac{1}{2}(\frac{\mathrm{Re}_T}{3})^{2/3} J^{1/3}$$
$$B^* = \frac{1}{2}(\frac{3}{\mathrm{Re}_T})^{1/3} J^{1/3} \tag{15}$$

so that we can finally obtain

$$\frac{u_s}{U} = A^*(\frac{d}{x})^{2/3} \approx \frac{1}{2}(\frac{\mathrm{Re}_T}{3})^{2/3} J^{1/3}(\frac{d}{x})^{2/3}$$
$$\frac{l}{d} = B^*(\frac{x}{d})^{1/3} = \frac{1}{2}(\frac{3}{\mathrm{Re}_T})^{1/3} J^{1/3}(\frac{x}{d})^{1/3} \tag{16}$$

If we use the axi-symmetric wake turbulent Reynolds number $\mathrm{Re}_{T=}$ 14.1 we can estimate $\frac{u_s}{U} = 1.4J^{1/3}(\frac{d}{x})^{2/3}$; $\frac{l}{d} = 0.3J^{1/3}(\frac{x}{d})^{1/3}$. The efficacy of these approximations to yield results consistent with transverse jet theory and measurements is described below.

C. Turbulence Model Parameter Estimates

Obviously, our focus in this document is to determine estimates for the turbulence model parameters constants $\{C_\mu, C_{\varepsilon 1}, C_{\varepsilon 1}\}$ which follow from a self-similar solution to the turbulence equations e.g. TKE:

$$U\frac{\partial k}{\partial x} = \frac{1}{y}\frac{\partial}{\partial y}(C_\mu y \frac{k^2}{\varepsilon}\frac{\partial k}{\partial y}) + C_\mu \frac{k^2}{\varepsilon}\left(\frac{\partial u}{\partial y}\right)^2 - \varepsilon \tag{17}$$

and the dissipation expression:

$$U\frac{\partial \varepsilon}{\partial x} = \frac{1}{y}\frac{\partial}{\partial y}(C_\mu \frac{k^2}{\varepsilon} y\frac{\partial \varepsilon}{\partial y}) + C_{\varepsilon 1}C_\mu k\left(\frac{\partial u}{\partial y}\right)^2 - C_{\varepsilon 2}\frac{\varepsilon^2}{k} = 0. \tag{18}$$

We introduce the near field self-similar formulations to give $k_s = CA^{*2}U^2 d^1 x^{-1}$ and $\varepsilon_s = D\frac{A^{*3}}{B^*}\frac{U^3}{d}d^2 x^{-2}$ to write:

$$\alpha(2g + \xi\frac{dg}{d\xi}) + \frac{1}{\xi}\frac{d}{d\xi}(\xi\frac{dg}{d\xi}) + \frac{1}{C}\left(\frac{df}{d\xi}\right)^2 - \mathrm{Re}_T\frac{D}{C}h = 0 \tag{19}$$

and

$$\alpha(4h + \xi\frac{dh}{d\xi}) + \frac{1}{\xi}\frac{d}{d\xi}(\xi\frac{dh}{d\xi}) + \frac{C_{\varepsilon 1}}{C}\left(\frac{df}{d\xi}\right)^2 - C_{\varepsilon 2}\,\mathrm{Re}_T\frac{D}{C}\frac{h^2}{g} = 0 \tag{20}$$

We will need to simplify either equation (19) or (20) to gain a solution. Utilizing the approximation that $\frac{g^2}{h} \approx \frac{g_0 g}{h} = 1$ which is consistent with both the Pope[1] and Tennekes and Lumley treatment[6] and the definition α = 1, we can write equation (19) as

$$(2g + \xi \frac{dg}{d\xi}) + \frac{1}{\xi}\frac{d}{d\xi}(\xi \frac{dg}{d\xi}) + \frac{1}{C}\left(\frac{df}{d\xi}\right)^2 - \mathrm{Re}_T \frac{D}{C} g_0 g = 0. \tag{21}$$

Now if we demand that $g_0 \mathrm{Re}_T \frac{D}{C} = 2$ the associated differential simplifies to become

$\xi \frac{dg}{d\xi} + \frac{1}{\xi}\frac{d}{d\xi}(\xi \frac{dg}{d\xi}) + \frac{1}{C}\left(\frac{df}{d\xi}\right)^2 = 0$ which can be integrated in closed form to give

$$g = \frac{1}{2C}\left(2E_{i\_1}(\frac{1}{2}\xi^2) - 2E_{i\_1}(\xi^2) - \exp(-\xi^2)\right), \tag{22}$$

where E_{i_1} is the exponential integral: $E_{i\_1}(x) = \int_x^\infty \frac{e^{-u}}{u} du$ This expression gives a solution for g(ξ) that honors the required boundary conditions: g' (0) = 0 and g(∞) = g(-∞) = 0. The constant $g_0 \mathrm{Re}_T \frac{D}{C} = 2$ was chosen because the associated solution honors the necessary boundary conditions, i.e. a solution for g(ξ) which is bounded for ξ>>1. Equation (22) also permits us to estimate g_0 to be $g_0 = \frac{1}{2}(g(0) + g(\infty)) = \frac{1}{4C}(2\ln(2) - 1)$. We emphasize that we have not imposed a magnitude for g(ξ) but have chosen an expression that provides a plausible solution for ξ→∞.

The proposed balance between the turbulent dissipation term and a portion of the mean flow convective term, i.e. $U\frac{\partial k}{\partial x} \propto \varepsilon$ is at first glance potentially troubling when viewed from our traditional notion of a local balance between production and dissipation. However, the energy budget for an axisymmetric wake measured by Uberoi and Freymouth[17] (discussed in Pope[1]) suggests that such is not the case. Indeed, their measurements suggest that

1. production is a rather small portion of the budget
2. dissipation is balanced by a partitioned component of the mean flow convective TKE, while,
3. turbulent transport balances the other component.

Similar results are noted for wake flows by Tennekes and Lumley[6]. These statements are recapitulated in our modeling approach whereby dissipation is balanced by a portion of the mean flow convection, $\mathrm{Re}_T \frac{D}{C} h = 2g$ with the other component balanced by the turbulent transport, i.e.: $\xi \frac{dg}{d\xi} + \frac{1}{\xi}\frac{d}{d\xi}(\xi \frac{dg}{d\xi}) + \frac{1}{C}\left(\frac{df}{d\xi}\right)^2 = 0$.

Returning to our analysis we note that there are now two algebraic expressions available to estimate the turbulent kinetic energy and dissipation as

$$\frac{D}{C_\mu C^2} = \mathrm{Re}_T \quad ; \quad \frac{2\ln(2)-1}{4C}\mathrm{Re}_T \frac{D}{C} = 2\,. \tag{23}$$

Eliminating $\frac{D}{C^2}$ from these expressions gives values for $C_\mu = \frac{8}{(2\ln(2)-1)}\mathrm{Re}_T^{-2} = 0.1$ and $\frac{D}{C^2} = C_\mu \mathrm{Re}_T = \frac{8}{(2\ln(2)-1)}\mathrm{Re}_T^{-1}$. Here we have utilized the axisymmetric wake Reynolds number estimate as $\mathrm{Re}_T = 14.1$, while noting that this value is consistent with the far-field wake and should be consider as preliminary.

We turn to the turbulent dissipation equation

$$4h + \xi\frac{dh}{d\xi} + \frac{1}{\xi}\frac{d}{d\xi}(\xi\frac{dg}{d\xi}) + \frac{C_{\varepsilon 1}}{C}\left(\frac{df}{d\xi}\right)^2 - C_{\varepsilon 2}\,\mathrm{Re}_T \frac{D}{C}\frac{h^2}{g} = 0\,. \tag{24}$$

We now use the same type of approximation to analyze equation (24). If we can write: $\frac{h^2}{g} = \frac{g_0 g}{g} h \approx g_0 h$ we can again demand that $C_{\varepsilon 2}\,\mathrm{Re}_T \frac{D}{C} g_0 = 4$ to honor a far field constraint on the self-similar dissipation h(ξ). Recalling that the TKE equation required $f(M)\,\mathrm{Re}_T\, g_0 \frac{D}{C} = 2$, we immediately (and unambiguously) compute an estimate for $C_{\varepsilon 2}$ with $C_{\varepsilon 2} = 2$. The value for $C_{\varepsilon 2}$ computed here is larger than the nominal value which is traditionally $C_{\varepsilon 2} = 1.92$. A final constraint follows from the solution to equation (24) which is simply Equation (22) with a modified magnitude, i.e.

$$h = \frac{C_{\varepsilon 1}}{2C}\left(2E_{i\_1}(\frac{1}{2}\xi^2) - 2E_{i\_1}(\xi^2) - \exp(-\xi^2)\right). \tag{25}$$

This solution then implies that $h_0 = C_{\varepsilon 1} = g_0$ whereby $C_{\varepsilon 1} = \frac{2\ln(2)-1}{4C}$.

Since our goal is to estimate the parameter $C_{\varepsilon 1}$ we will require an estimate for the constant C which is associated with the TKE magnitude. Recalling that $k_s = Cu_s^2$ we can estimate k_s by utilizing the so-called Bradshaw assumption[1,6,8] namely that $u'v' = \frac{2}{3}(0.45)k_s = 0.3k_s$. Then employing: $u'v' \approx \frac{u_s^2}{\mathrm{Re}_T} f'$ with $f' = \frac{1}{2}(f'_{\max} + f'(\infty)) \approx \frac{0.62}{2} = 0.31$ (a simple arithmetic average for the distribution) we can estimate

$C = \frac{k_s}{u'v'} \approx \frac{3}{2(0.45)} \mathrm{Re}_T^{-1}(0.31)$. Using $\mathrm{Re}_T = 14.1$ we find that $C \approx 0.072$. The estimate for $C_{\varepsilon 1}$ then follows as: $C_{\varepsilon 1} = g_0 = \left(\frac{2\ln(2)-1}{4(0.072)} \right) \approx 1.34$.

To summarize the turbulence parameter estimates are:

$$C_\mu = 0.1, \qquad C_{\varepsilon 2} = 2, \text{and} \qquad C_{\varepsilon 1} = 1.34 \tag{26}$$

We will refer to $\{C_\mu, C_{\varepsilon 2}, C_{\varepsilon 1}\}$ computed using Equation (26) as C_a.

D. Jet Trajectory Formulation Explicitly Using Analytical Turbulence Model Parameters

A common description of the jet-in-crossflow behavior is the jet penetration trajectory[25, 26]. Simplified models have been developed based on line-impulse, counter-rotating vortex pair expressions. They provide good estimates for trajectory behavior[26,27]. The formulation of these models directly involves turbulence behavior through their length scale definition, implying that one can expect that turbulence model parameter information can be explicitly related to the trajectory behavior. Here we utilize the approximate analytical descriptions of the self-similar jet in crossflow to formulate a jet trajectory model that directly includes a subset of the turbulence model parameter constants.

We start by examining the trajectory model formulation. We can relate the local turbulence behavior of the jet to the trajectory via a line impulse vorticity argument. The fundamental expression that is used is the vertical velocity *W* induced by a CVP[12] as

$$W = \frac{dz}{dt} = \frac{\Gamma}{4\pi L} \tag{27}$$

where 2L is the spacing between the vortices and Γ is the circulation strength of the vortex. We can relate the circulation back to the jet strength as

$$\frac{\pi}{4}\rho_j V_j^2 d^2 = 2\rho_\infty U \Gamma L. \tag{28}$$

We then connect the nozzle impulse per unit length $\frac{\frac{\pi}{4}\rho_j V_j^2 d^2}{U}$ to the impulse per unit length, say p', of the CVP via the impulse-circulation expression: $p_z' = 2\rho_\infty \Gamma L$ [28,29]. The distance separating the vortices, L, is slightly less than the jet spreading distance[16] and estimated to be $0.7\,l \le L \le 0.8l$, with an average value of $L = \frac{3}{4}l$. However, a useful limiting case to consider is to assume that $L = l$ i.e. the vortex core is equal to spreading location.

Clearly the turbulent length scale specification is the connection between turbulence model and the jet penetration trajectory, where the trajectory differential equation is

$$U\frac{dz}{dx}=\frac{\frac{\pi}{4}\rho_j V_j^2 d^2}{\frac{U}{8\pi\rho_\infty L^2}}\rightarrow\frac{dz}{dx}=\frac{1}{32}J(\frac{L}{d})^{-2}. \tag{29}$$

Similarly, the vortex speed model $W=\frac{dz}{dt}=\frac{\Gamma}{4\pi L}$ is also related to the turbulence length scale via

$$\frac{\Gamma}{Ud}=\frac{\pi}{8}J(\frac{L}{d})^{-1}=\frac{\pi}{8}J(\frac{l}{d})^{-1}. \tag{30}$$

We now derive expressions for $\frac{l}{d}$ as a function of the turbulence model parameters.

The turbulence modeling formulation involves specification of the velocity and length scales $u_s=A^*Ud^{2/3}x^{-2/3}$; $l=B^*d^{2/3}x^{1/3}$ (far-field) whereby the turbulent kinetic energy and dissipation follow from the definitions as $k_s=CA^{*2}U^2d^{4/3}x^{-4/3}$ and $\varepsilon_s=D\frac{A^{*3}}{B^*}\frac{U^3}{d}d^{7/3}x^{-7/3}$ which were developed previously for the classical far-field analysis. The turbulent length and velocity scale constants A^* and B^* are related via:

$$\frac{B^*}{3A^*}\mathrm{Re}_T=1\quad;\quad A^*B^{*2}=\frac{J}{8}, \tag{31}$$

to give $A^*=\frac{1}{2}(\frac{\mathrm{Re}_T}{3})^{2/3}J^{1/3}$; $B^*=\frac{1}{2}(\frac{3}{\mathrm{Re}_T})^{1/3}J^{1/3}$, so that

$$\begin{aligned}\frac{u_s}{U}&=A^*(\frac{d}{x})^{2/3}=\frac{1}{2}(\frac{\mathrm{Re}_T}{3})^{2/3}J^{1/3}(\frac{d}{x})^{2/3}\\ \frac{l}{d}&=B^*(\frac{x}{d})^{1/3}=\frac{1}{2}(\frac{3}{\mathrm{Re}_T})^{1/3}J^{1/3}(\frac{x}{d})^{1/3}\end{aligned} \tag{32}$$

The self-similar turbulent velocity and length scale constants A and B, respectively, must now be related to the turbulence model parameters. The turbulence model parameters are contained within the definition for the constant turbulent Reynolds number Re_T since

$$\frac{D}{C_\mu C^2}=\mathrm{Re}_T. \tag{33}$$

To proceed we require two additional expressions to estimate D and C. The turbulence model parameter procedure developed previously utilizes the two approximations $C=\frac{1}{4}(\frac{2\ln 2-1}{C_{\varepsilon 1}})$ and

$$\frac{1}{4}(2\ln 2-1)C_{\varepsilon 2}\frac{D^2}{C^4}=4 \tag{34}$$

The resulting solution for D is

$$D = \frac{1}{4}(2\ln 2 - 1)\frac{C_\mu^{1/2}}{C_{\varepsilon 2}^{1/2} C_{\varepsilon 1}^2}, \tag{35}$$

whereby the Reynolds number is

$$\mathrm{Re}_T = \frac{4}{(2\ln 2 - 1)^{1/2}} C_\mu^{-1/2} C_{\varepsilon 2}^{-1/2}. \tag{36}$$

The associated length scale expression $\frac{l}{d} = B^*(\frac{x}{d})^{1/3} = \frac{1}{2}(\frac{3}{\mathrm{Re}_T})^{1/3} J^{1/3}(\frac{x}{d})^{1/3}$ is now

$$\frac{l}{d} = \frac{1}{2}\left(\frac{3}{4}(2\ln 2 - 1)^{1/2} C_\mu^{1/2} C_{\varepsilon 2}^{1/2} J(\frac{x}{d})\right)^{1/3}. \tag{37}$$

It is convenient to write this expression as $\frac{l}{d} = \frac{1}{2}\left(\frac{3}{4}(2\ln 2 - 1)^{1/2} C_\mu^{1/2} C_{\varepsilon 2}^{1/2} J(\frac{x}{d})\right)^{1/3}$. The trajectory differential equation $\frac{dz}{dx} = \frac{1}{32} J(\frac{l}{d})^{-2}$ is then integrated to give

$$\begin{aligned} \frac{z}{d} &= \frac{3}{8}\left(\frac{16}{9}\frac{C_\mu^{-1} C_{\varepsilon 2}^{-1}}{(2\ln 2 - 1)} J(\frac{x}{d})\right)^{1/3} \\ &\approx 0.624[C_\mu C_{\varepsilon 2}]^{-1/3} J^{1/3}(\frac{x}{d})^{1/3} \end{aligned} \tag{38}$$

Equation (38) expresses a simple trajectory model as a function of the associated turbulence model parameters specifically C_μ and $C_{\varepsilon 2}$. Below, we compare it to numerical solution, as well as other analytical models of jet penetration.

III. Comparison to Computational Approaches

The preceding approximate analytical development has focused on estimating the main parameters within the k-ε turbulence model. While the approach utilized here is highly simplified it nonetheless provides parameter estimates for the major model parameters $C_a = \{C_\mu, C_{\varepsilon 2}, C_{\varepsilon 1}\}$. With access to the turbulence model parameters it is possible to perform a computational study of an experimentally well-characterized jet-in-crossflow problem to ascertain the efficacy of the analytically estimated turbulence model parameters. Further, one may use the analytical model for jet penetration as a check on the accuracy of the self-similar model from which C_a was derived.

A. RANS Computational Study Utilizing Analytical Parameters

Values of C_a were used to perform RANS (k-ε) simulations of jet-in-crossflow (JIC), with a jet-to-freestream momentum ratio *J* of 10.2. The freestream velocities for the three cases are 215, 251 and 286 m/s respectively, corresponding to freestream Mach number $M = 0.6, 0.7$ and 0.8. We used experimental data from Beresh et al[16] to

validate these RANS simulations. A schematic of the experimental setup is in Figure 1 (left). A Mach 3.73 jet is introduced into a freestream of Mach number M, flowing from left to right. The jet curves with the flow and rolls into a counter-rotating vortex pair (CVP) as it flows downstream. PIV measurements of the mean flow are available on the midplane (plane of symmetry) and for the M = 0.8 case, also on the crossplane that slices through the CVP. Figure 1 (right) shows the streamwise vorticity field on the crossplane; the CVP is clearly visible. A window $\mathcal{W}$ is delineated around one of the vortices for clarity. The RANS simulations are performed with a compressible form of the RANS equations[21,22]; a description of the governing equations and the implicitly stepped finite volume numerical method used to solve them is available in Ray et al[2]. The mesh requires about 10 million grid cells to obtain grid-independent solutions[20]. Velocities on the midplane (vertical and streamwise) are extracted at three streamwise locations (at x/d = 21, 31.5 and 42, where d = 9.53 mm is the diameter of the jet) and compared against experimental measurements from Beresh et al[16].

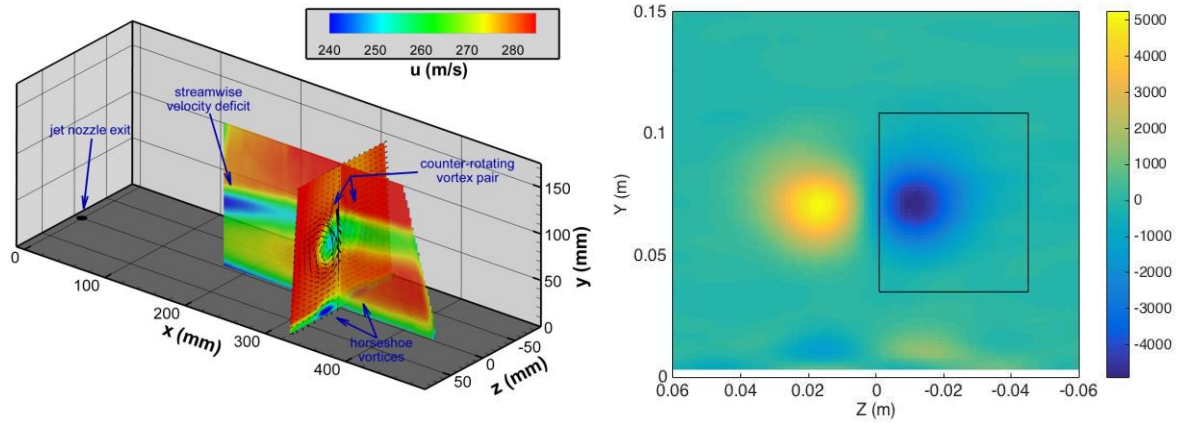

Figure 1 Left: Schematic of the wind tunnel section simulated in this paper. The freestream is introduced from the left. The jet is at the bottom of the test section. The midplane and crossplane are clearly shown. Right: The counter-rotating vortex pair (CVP) of the jet as seen on the crossplane. The window in black delineates one of the vortices.

In Figure 2, we plot the streamwise velocity deficit (top row) and the normalized vertical velocity (bottom row) at the three streamwise locations mentioned above for the M = 0.8 interaction. Here, streamwise velocity deficit is defined as (U – u) / U, where U is the maximum velocity encountered at a streamwise location, and is typically slightly higher than the freestream velocity because of the mass added by the jet. Experimental data are plotted as symbols and the predictions using $C_{nom} = \{C_\mu, C_{\varepsilon 2}, C_{\varepsilon 1}\} = \{0.09, 1.92, 1.44\}$[30], the nominal value of the parameters, with a dashed line. Predictions using C_a are plotted with a solid line. The improvements over predictions using C_{nom} are clear and quite significant. The flowfield obtained with C_{nom} contains a CVP that is too strong, as seen in the vertical velocity induced by it (bottom row of figures); further, the CVP penetrates excessively into the crossflow, compared to the experimental results. The use of C_a largely corrects these errors at all the streamwise locations; in fact, the experimental measurements are very close to the C_a predictions. The same improvements in predictive skill are seen in Figure 3, which plots the results for the M = 0.7 case.

Figure 4 plots the results for the M = 0.6 case. C_{nom} provides very poor predictions of the experimental measurements, and the use of C_a does result in an improvement. However, the quality of agreement between C_a and the experimental results is not as good as in Figure 2 and Figure 3. This could be due to the approximate nature of the derivation of C_a, though the experimental measurements for M = 0.6 also show some anomalous behavior compared to M = 0.7 and M = 0.8. For example, between $2 \leq y/d \leq 7$ the streamwise velocity deficit seems to adopt a constant value for M = 0.6, whereas in M = 0.7 and M = 0.8, it reduces to zero. In contrast, the numerical predictions of the streamwise velocity deficit for M = 0.6, as in the M = 0.7 and 0.8, do reduce to zero outside the CVP.

In Figure 5 we plot the streamwise vorticity field on the crossplane. The vorticity predicted by C_{nom} and $C_{a,}$ are plotted in color, with the vorticity computed from PIV measurements plotted on top as contours. This is done for the M = 0.8 case, for which we have PIV measurements on the crossplane[23]. We see (from the color map) that the use of

C_a weakens the CVP and shrinks it size, thus bringing it in line with experimental data. It also sits somewhat below the experimental CVP, which can also be seen in the midplane velocity profiles in Figure 2.

In Figure 6 we compare the vorticity fields plotted in Figure 5 quantitatively. We compute the circulation of vorticity field inside $\mathcal{W}$, as well as the centroid of that distribution in the crossplane (henceforth referred to as the "point-vortex metrics"). This is done for flowfields generated by C_{nom} and $C_{a,}$ as well as the flowfield that was measured via PIV. The point-vortex metrics of the simulated flowfields are normalized by their experimental counterparts and plotted in Figure 6. The horizontal line indicates a perfect match. It is clear that the circulation of the CVP simulated using C_a matches experiments very well, whereas C_{nom} leads to a CVP that is about 30% too strong. This explains the excessive vertical velocities seen in Figure 2. The CVP's height predicted by C_a is also close to experimental results, whereas C_{nom} provides a CVP that is about 30% too high. This is also seen in the plots for streamwise velocity deficit in Figure 2. The figure also shows that CVP simulated using C_a is too close to the midplane, though the difference is small (about 10%). Due to this small difference, it was not readily apparent in Figure 5.

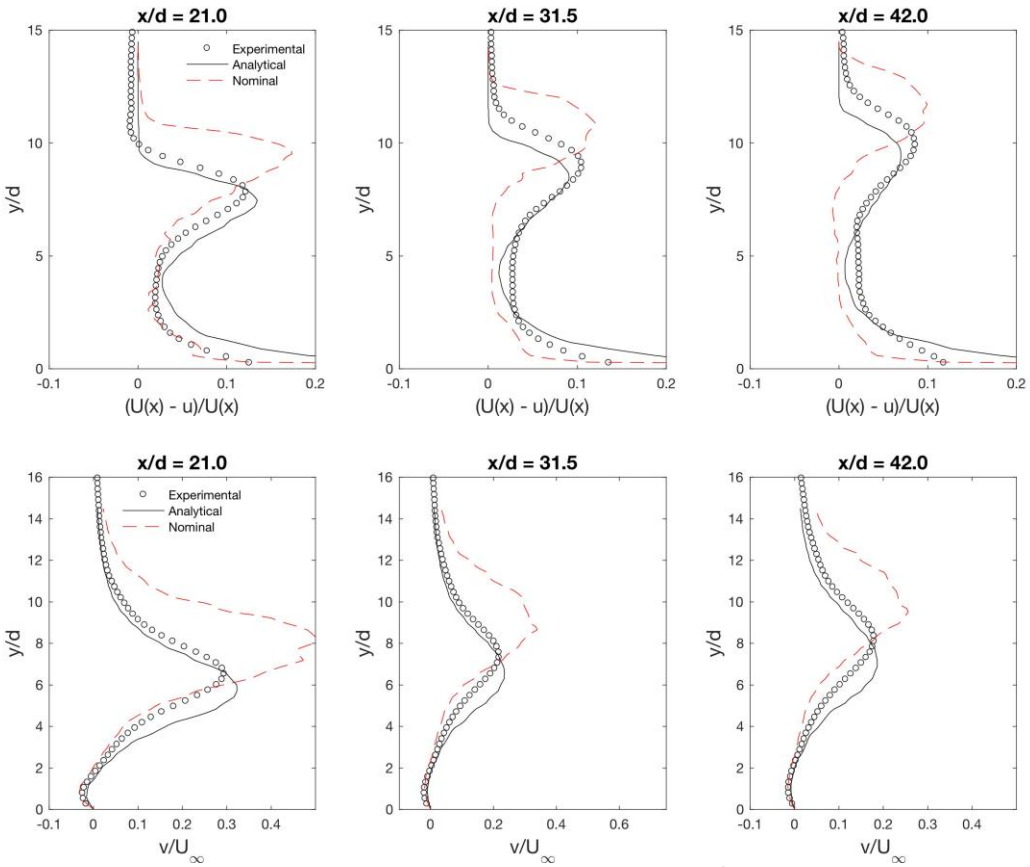

Figure 2 Top row: Plots of streamwise velocity deficit at three streamwise locations $\boldsymbol{x/d = 21, 31.5}$ and $\mathbf{42.0}$. Experimental data are plotted with symbols, the RANS predictions using the nominal parameter values C_{nom} are plotted with a dashed line and those obtained using C_a with a solid line. Bottom row: The normalized vertical velocity $\boldsymbol{v/U_\infty}$. Results are for the M = 0.8 test case.

Having established that the CVP simulated using C_a is far more accurate than the one generated using C_{nom}, we investigate the finer points of the simulated jet versus experiments. The evolution of the jet can be tracked using the streamwise velocity deficit, the maximum vertical velocity on the midplane or the CVP; they do not exactly coincide spatially. In Figure 7 (left) we plot the streamwise velocity deficit (in color) as computed using C_a, with the streamwise vorticity overlaid with contours. In Figure 7 (right) we illustrate the experimental counterpart. We see that the simulated jet is slightly below the experimental one, as seen in Figure 2. It is also slightly narrower. The CVP is also closer to the midplane, and occupies a greater fraction of the region where the streamwise velocity deficit assumes significant values. This could be a consequence of having a narrower jet. However, given that C_a

was estimated under a set of gross assumptions required for a self-similar solution, it is surprising that it does so well for JIC simulations.

In

Table **1** we compare the analytically-derived C_a against the parameters estimated via the Bayesian parameter estimation approach[2]. It was computed using the same experimental data and RANS equations. We compare the values of $C_\mu, C_{\epsilon 2}$ and $C_{\epsilon 1}$that correspond to C_{nom}, C_a, and C_{opt}, where $C_{opt}$is the MAP (maximum a posteriori) estimate obtained by the Bayesian calibration performed for a M = 0.8 crossflow. The results indicate that C_a is in good agreement with the Bayesian results. While we emphasize that the current result is highly simplified, the good agreement between approaches suggests that the data-informed procedure described by Ray et. al.[2,3,4,5] likely succeeds because it honors the underlying physics associated with the jet-in-crossflow problem. It also suggests that compressibility effects at these downstream locations are weak, since our incompressible formulation provides relatively good agreement with experimental data. By offering more than a strictly semi-empirical modification, flow-specific calibration would then appear to be a useful procedure to develop dedicated simulation tools for a particular problem class.

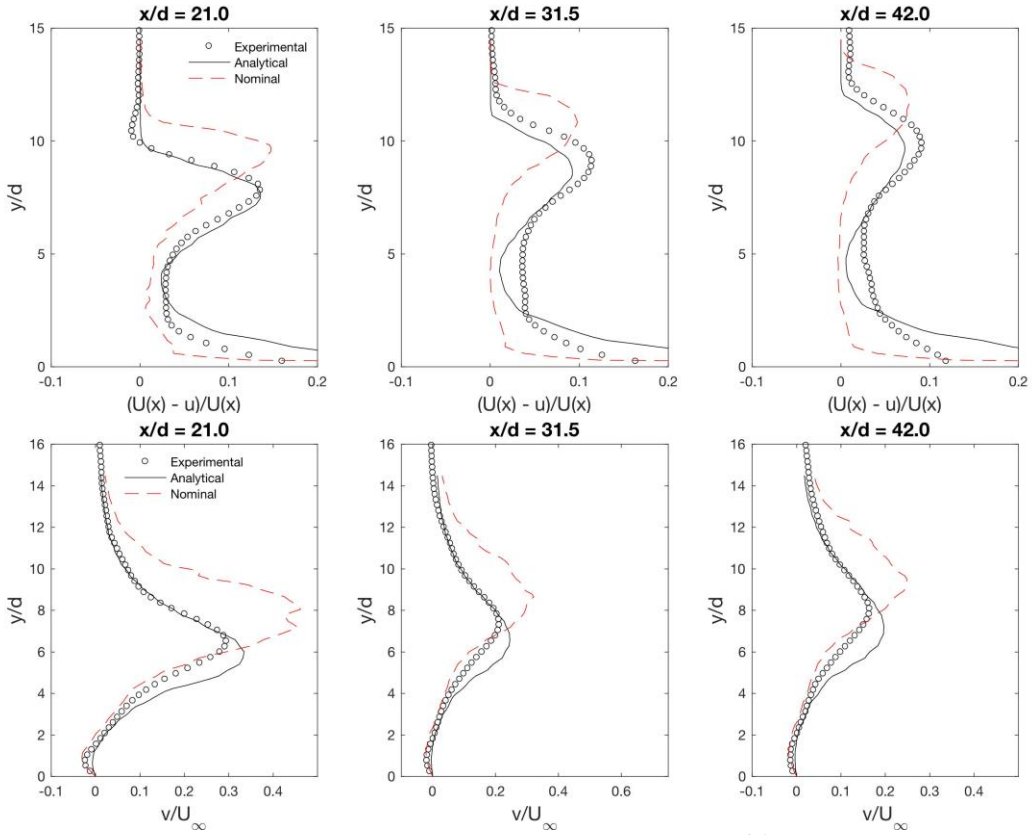

Figure 3 Top row: Plots of streamwise velocity deficit at three streamwise locations $\boldsymbol{x/d} = \mathbf{21}, \mathbf{31.5}$ and $\mathbf{42.0}$. Experimental data are plotted with symbols, the RANS predictions using the nominal parameter values C_{nom} are plotted with a dashed line and those obtained using C_a with a solid line. Bottom row: The normalized vertical velocity $\boldsymbol{v/U_\infty}$. Results are for the M = 0.7 test case.

The agreement between jet-in-crossflow calibrated models, however, comes at a price regarding other flow effects. A wall-bounded shear layer would be expected to honor traditional log law behavior[1] which in turn imposes a well know constraint[1,8] upon the k-ε constants as

$$\kappa^2 = (C_{\varepsilon 2} - C_{\varepsilon 1})\sigma_\varepsilon C_\mu^{1/2} \tag{39}$$

where κ = 0.41 is the Von Karman constant. Utilizing the so-called nominal constants i.e., $C_{\varepsilon 2} = 1.92$, $C_{\varepsilon 1} = 1.44$, $C_{\mu} = 0.09$ and $\sigma_{\varepsilon} = 1.3$ we estimate that κ≈0.43 which compares well to the classical value. Utilizing values that are optimized for the jet-in-crossflow problem, i.e., $C_{\varepsilon 2} = 2.0$, $C_{\varepsilon 1} = 1.34$, $C_{\mu} = 0.1$ and $\sigma_{\varepsilon} = 1.0$ yields: κ ≈ 0.46 which is 15% larger as compared to the expected value. Analytical constraints that explicitly require production versus dissipation invariance such as for a homogeneous shear flow[1] lead to

$$\frac{P}{\varepsilon} = \frac{C_{\varepsilon 2} - 1}{C_{\varepsilon 1} - 1}, \tag{40}$$

where $\frac{P}{\varepsilon}$ is measured as 1.7 Nominal results give $\frac{C_{\varepsilon 2} - 1}{C_{\varepsilon 1} - 1} = \frac{1.92 - 1}{1.44 - 1} = 2.1$ which is larger than the experimentally measured value. Utilization of the current incompressible values gives $\frac{C_{\varepsilon 2} - 1}{C_{\varepsilon 1} - 1} = \frac{2 - 1}{1.34 - 1} = 2.94$ which is much too large. These two examples tend to demonstrate our contention that calibration for turbulence model coefficients is necessarily problem-class dependent.

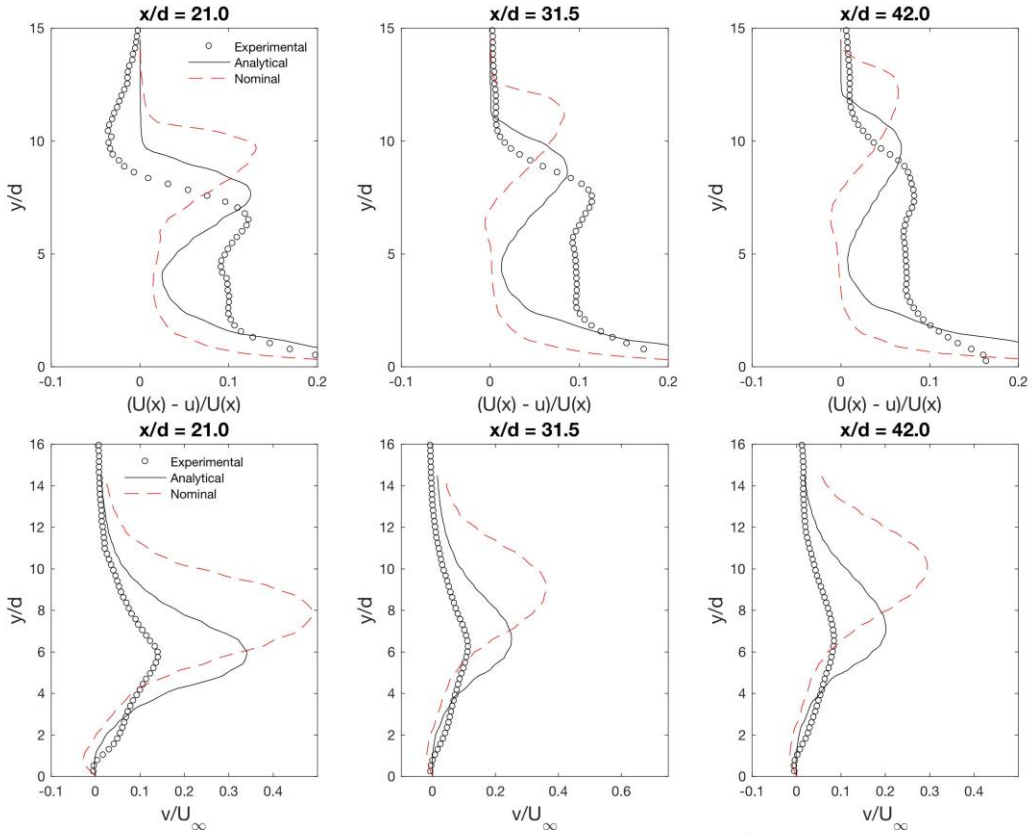

Figure 4 Top row: Plots of streamwise velocity deficit at three streamwise locations $\boldsymbol{x/d} = \mathbf{21}, \mathbf{31.5}$ and $\mathbf{42.0}$. Experimental data are plotted with symbols, the RANS predictions using the nominal parameter values C_{nom} are plotted with a dashed line and those obtained using C_a with a solid line. Bottom row: The normalized vertical velocity $\boldsymbol{v/U_{\infty}}$. Results are for the M = 0.6 test case.

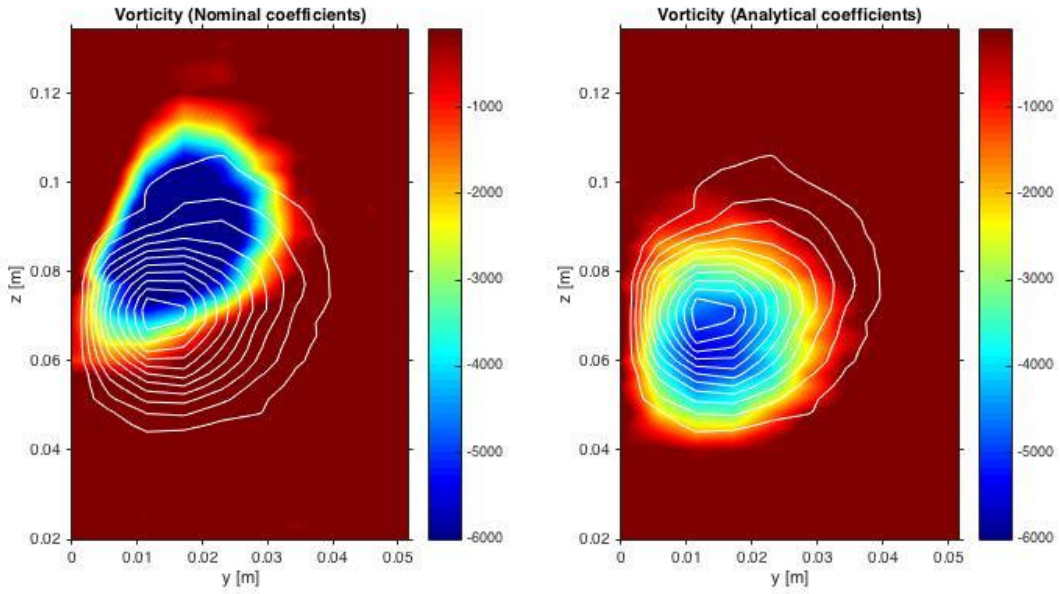

Figure 5 Vorticity plots inside the window $\mathcal{W}$. Left: Vorticity predictions using C_{nom} are plotted in color, with the experimental vorticity field overlaid as white contour lines. Right: Vorticity predicted using C_a. Results are for the M = 0.8 case.

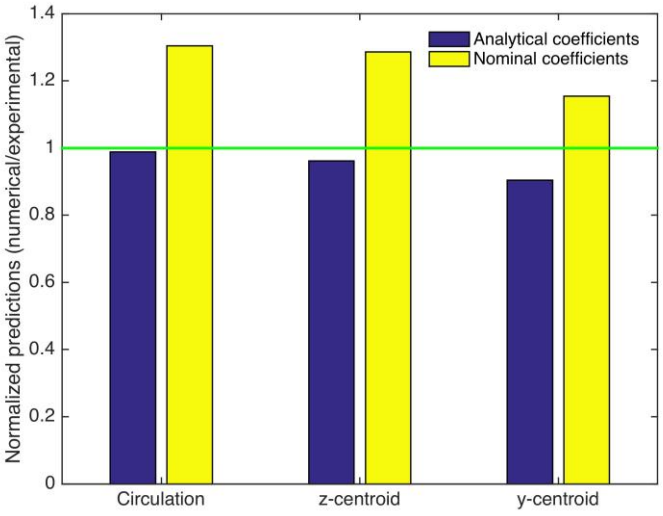

Figure 6 Circulation and position of the centroid of the CVP computed using C_a (analytical coefficients) and C_{nom} (nominal coefficients). The quantities are normalized by their experimental counterparts. The horizontal line indicates perfect agreement.

Table 1. Comparison between the current incompressible, self-similar model, the compressible Bayesian model of Ray et. al.[2] and the nominal model, suggesting relatively good agreement between the current model and the calibrated one. "B" is used as shorthand for the parameter values obtained using Bayesian calibration. "N" is the corresponding shorthand for nominal parameters.

	C_μ	$C_{\epsilon 1}$	$C_{\epsilon 2}$
Self-Similar Model (current) (C_a, M = 0)	0.10	1.34	2.00
Bayesian Model (C_{opt}, M = 0.8)	0.10	1.42	2.10
Relative Error ($SS_{M=0}$ - B) / B (%)	0%	-6%	-5%
Nominal (C_{nom})	0.09	1.44	1.92
Relative Error (SS - N) / N (%)	11%	-7%	4%

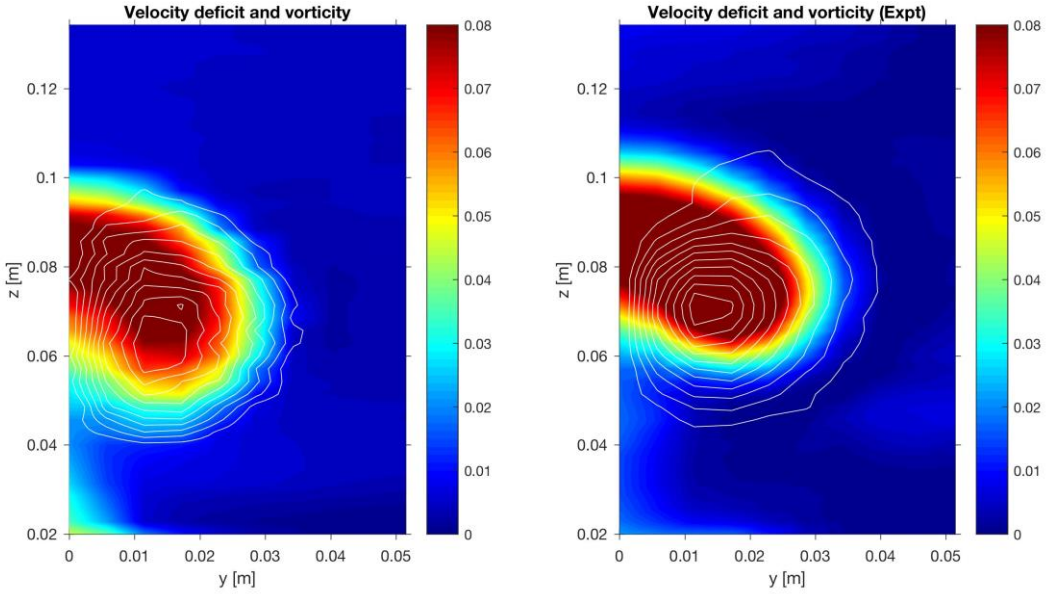

Figure 7 Plots of streamwise velocity deficit (in color) with the vorticity plotted on top with contours. Left: results simulated using C_a. Right: Experimental results. As seen in Figure 2 and Figure 5, the simulated jet sits a little lower than the experimental one and is also a little narrower.

B. Assessing the Jet Trajectory Model

We now evaluate the impact of C_{nom}, C_a and C_{opt} on jet penetration (Equation 38). Specifically, we estimate $Z = 0.624\ (C_\mu\ C_{\epsilon 2})^{-1/3}$ for these values of C and tabulate in Table 2. We see that Equation 38 predicts that C_{nom} will result in excessive jet penetration, as observed in Figures 2-5, vis-à-vis C_a. It will also result in penetrations larger than C_{opt}, as seen in Ref. 2. However, the impact, as estimated via Equation 38, is not very large (though it does have the correct trend) and with access to RANS simulations we can directly estimate the trajectory penetration without being constrained to the functional form associated with Equation (38).

Table 2. Comparison between the trajectory function constants as a function of k-ε turbulence model parameters using the current incompressible, self-similar model (C_a), Bayesian-calibrated (C_{opt}) and nominal values (C_{nom}). Notice that the nominal values result in an increased degree of penetration relative to the self-similar and calibrated parameters which is consistent with the vortex pair locations in Figure 5. $Z = 0.624\ (C_\mu\ C_{\epsilon 2})^{-1/3}$

	C_μ	$C_{\epsilon 1}$	$C_{\epsilon 2}$	Z	$\frac{(Z_{nom}-Z)}{Z_{nom}}$ (%)
Self-Similar Model (C_a, M = 0)	0.10	1.34	2.00	1.06	5.2
Bayesian Model (C_{opt}, M = 0.8)	0.10	1.42	2.10	1.04	6.7
Nominal (C_{nom})	0.09	1.44	1.92	1.11	0

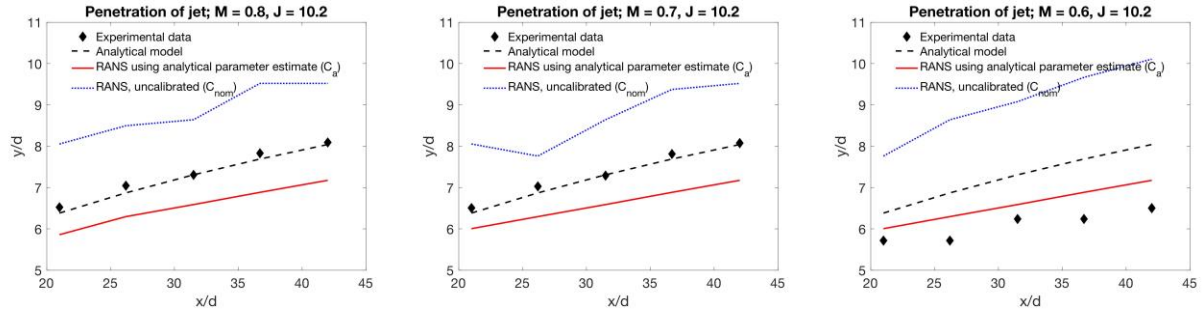

Figure 8. Comparison of jet penetration trajectories predicted using the analytical model i.e., Equation (38) with $\boldsymbol{C_a}$ and RANS computations using both $\boldsymbol{C_a}$ and $\boldsymbol{C_{nom}}$. Results are plotted for crossflow Mach number M = 0.8 (left), M = 0.7 (middle) and M = 0.6 (right). The symbols denote experimental results, the dotted lines the RANS simulation using $\boldsymbol{C_{nom}}$, and the solid lines the RANS simulations using $\boldsymbol{C_a}$. Equation (38) is plotted using dashed lines.

In Figure 8, we plot the trajectory of the jet computed using Equation 38 (with C_a), and compare it with RANS simulations performed with C_a and C_{nom}. The subfigure on the left plots results for a M = 0.8 crossflow. In the middle and right subfigures, results are plotted for M = 0.7 and 0.6. In the RANS simulations, the jet penetration at any streamwise location is computed to be where the vertical velocity achieves its maximum value. We see that Equation 38 compares well with the RANS results for M = 0.8 and M = 0.7. The analytical model seems to provide a better match to the experimental values than the RANS simulation for the M = 0.7 and M = 0.8 cases. However, the agreement may be fortuitous, as it does not hold for M = 0.6. Equation (38) is perhaps better used as a relative measure of the trajectory behavior and a useful delineation of the functional behavior of the turbulence model parameters, as opposed to an absolute predictive tool. Therefore, there is value in comparing the results of the current model to a family of "classical" e.g. Hasselbrink and Mungal[26], Margarson[31] and Pratte and Baines[32] jet penetration trajectory models. All of these models have the same basic analytical form as: $\frac{z}{d} \approx A_0 J^{1/3} (\frac{x}{d})^{1/3}$ and permit direct comparison in Table 3.

Table 3. Simplified jet trajectory function magnitude constant A_0. Most classical result suggest a greater degree of jet penetration than observed in the Beresh[16] experiment, while the estimates based upon the self–similar constants are significantly reduced.

Trajectory Coefficient; A_0, $\frac{z}{d} \approx A_0 J^{1/3} (\frac{x}{d})^{1/3}$	Reference
$A_0 = 1.60$	Hasselbrink and Mungal[26]
$A_0 = 1.60$	Margarson[31]
$A_0 = 2.05$	Pratte and Baines[32]
$A_0 = 1.06$	Equation (38), using C_a

To summarize, the analytical derived self-similar turbulence model parameters $C_a = \{C_\mu, C_{\epsilon 1}, C_{\epsilon 2}\} = \{0.1, 1.34, 2.0\}$ have been utilized in RANS computations and compared to the well characterized experiment by Beresh et. al.[16]. The use of the analytically estimated in the computations yields improved comparison with the experimental measurements. A direct connection between traditional jet in crossflow penetration trajectory models and the turbulence models is exploited to also demonstrate the efficacy of the analytically estimated coefficients.

IV. Conclusion

In this paper, we have developed a simplified, analytical, similarity-based model for axi-symmetric wake/jet behavior in a crossflow that is then used to estimate values for the supporting turbulence model coefficients. The resulting estimates for the turbulence model parameters are in general agreement (less than 10% relative error) with the calibrated results of Ray et. al.[2] Numerical simulations performed with the analytically estimated parameters are in good agreement with experimental measurements that cover a range of freestream Mach numbers. They are far better than the predictions obtained using C_{nom}, the nominal values of the parameters. Predictions of velocity on the midplane as well as vorticity on the crossplane were used to validate the analytical parameter estimates. The model was also parlayed into an expression for the jet's penetration into the crossflow, which showed good agreement with experimental and RANS simulations. It also explained the over-prediction of jet penetration by RANS simulations using C_{nom}. The superiority of C_a over C_{nom}, even though derived from an analytically simplified solution of a jet-in-crossflow problem, leads us to believe that the predictive skill of RANS can be significantly enhanced (over those obtained using C_{nom}) by using appropriate parameter values e.g., those obtained via calibration. Our previous paper[2] explored this possibility.

A drawback for our previous Bayesian calibration approach was that it was purely data-driven, without any theoretical justification. There was also the risk that the calibrated values were also compensating for the model-form error (i.e., approximations in the physical modeling of turbulence) that is inherent in RANS. The close agreement between the turbulence model coefficients obtained from Bayesian calibration and the analytically estimated values estimated in this paper suggest that the calibration approach is far more capable than simple data-dependent regression, and is firmly rooted in the underlying physical description. It attests to the credibility of results drawn from Bayesian calibration. A future paper will investigate calibration in depth i.e., across multiple freestream Mach numbers and check how they compare to predictions using C_a obtained using Equation (26). Calibrating a RANS model requires a significant amount of effort and we will also check whether C_a may be used as a compromise between C_{nom} and rigorously calibrated parameter values.

V. Acknowledgements

Sandia is a multiprogram laboratory operated by Sandia Corporation, a Lockheed Martin Company, for the United States Department of Energy's National Nuclear Security Administration under Contract DE-AC04-94AL85000.

VI. References

[1]Pope, S. B., *Turbulent Flows*, Cambridge U. Press, Cambridge, UK, 2000.

[2]Ray, J., Lefantzi, S., Arunajatesan, S., DeChant, L. "Bayesian Parameter Estimation of a k-ε Model for Accurate Jet-in-Crossflow Simulations", *AIAA Journal*, 54(8): 2432-2448, 2016, February 2016.

[3]Ray, J., Lefantzi, S., Arunajatesan, S., and DeChant, L. "Learning an Eddy Viscosity Model with Shrinkage - A Case Study with Jet-in-Crossflow Configuration", under review, *ASME/ASCE Journal of Risk and Uncertainty in Engineered Systems*.

[4]Ray, J., Lefantzi, S., Arunajatesan, S., and DeChant, L. "Bayesian Calibration of a RANS Model with a Complex Response Surface - A Case Study with Jet-in-Crossflow Configuration", 45 AIAA Fluid Dynamics Conference, Dallas, TX, June 22-26, 2015. Conference paper: AIAA-2015-2784.

[5]Ray, J., Lefantzi, S., Arunajatesan, S., and DeChant, L., "Bayesian Calibration of a k-ε Turbulence Model for Predictive Jet-in-Crossflow Simulations", 44th AIAA Fluid Dynamics Conference, Atlanta, GA, June 16-20, 2014. Conference paper: AIAA-2014-2085.

[6]Tennekes, H., Lumley, J., *A First Course in Turbulence*, MIT Press, Cambridge, MA, 1987.

[7]Anderson, D., Tannehill, J. Pletercher, R., *Computational Fluid Mechanics and Heat Transfer*, Hemisphere, NY, 1984.

[8]Wilcox, D., *Turbulence Modeling for CFD*, DCW Industries, Anaheim, CA, 2002.

[9]Davidson, P. A., *Turbulence, An Introduction for Scientists and Engineers*, Oxford, Oxford, UK, 2004.

[10]Georgiadis, N., Yoder, D., "Recalibration of the Shear Stress Transport Model to Improve Calculation of Shock Separated Flows," AIAA-2013-0685.

[11]Sarkar, S., Erlenbacher, G., Hussaini, M. Y., Kreiss, H. O. "The Analysis and Modeling of Dilatational Terms in Compressible Turbulence," NASA-CR-181959, 1989.

[12]Zeman, O., "Dilatational Dissipation: the Concept and Application in Modeling Compressible Mixing Layers," *Physics of Fluids A*, 2, 2, pp.178-188. 1991

[13]Guillas, S., Glover, N., Malki-Epshtein, L., "Bayesian Calibration of the Constants of the k-ε Turbulence Model for a CFD Model of Street Canyon Flow, *Computer Methods in Applied Mechanics and Engineering*, 279, 1, pp. 536-553, 2014.

[14]Broadwell, J. E., Breidenthal, R. E., "Structure and Mixing of a Transverse Jet in Incompressible Flow," *JFM*, 454, pp 113-144, 1984.

[15]Mahesh, K., "The Interaction of Jets with Crossflow," *Annual Review Fluid Mechanics*, 45, pp. 379-407, 2013.

[16]Beresh, S. J., Henfling, J. F., Erven, R. J., and Russell W. Spillers, R. W. "Penetration of a Transverse Supersonic Jet into a Subsonic Compressible Crossflow", *AIAA Journal*, Vol. 43, 2, pp. 379-389, 2005.

[17]Uberoi1, M., FreyMuth, P., "Turbulent Energy Balance and Spectra of the Axisymmetric Wake, *Phys. Fluids* 13, 2205, 1970

[18]Lee, J., Chu, H. *Turbulent Jets and Plumes: a Lagrangian Approach*, Kluwer, Boston 2003.

[19]Greitzer, E., Tan, C., Graf, M., *Internal Flow: Concepts and Applications*, Cambridge, Cambridge, UK, 2007.

[20]Arunajatesan, S., "Evaluation of Two-Equation RANS Models for Simulation of Jet-in-Crossflow Problems," 50th AIAA Aerospace Sciences Meeting, 2012. Conference paper: AIAA-2012-1199.

[21]Brinckman, K. W., Calhoon, W. H., Dash, S. M., "Scalar Fluctuation Modeling for High-Speed Aeropropulsive Flows", AIAA Journal_, Vol. 45, No. 5, 2007, pp. 1036-1046

[22]Papp, J. L., Dash, S. M., "Turbulence Model Unification and Assessment for High-Speed Aeropropulsive Flows", 39th AIAA Aerospace Sciences Meeting and Exhibit, 2001, http://arc.aiaa.org/doi/10.2514/1.J054758

[23]Beresh, S. J., Henfling, J. F., Erven, R. J., and Spillers, R. W., "Crossplane velocimetry of a transverse supersonic jet in a transonic crossflow," AIAA Journal, Vol. 44, No. 12, 2006, pp. 3051–3061.

[25]Durando, N., Vortices Induced in a Jet by Subsonic Crossflow, *AIAA Journal*, 9, pp 325-327, 1971.

[26]HasselBrink, E. F., Mungal, M. G., "Transverse Jets and Flames. Part 1, Scaling Laws for Strong Transverse Jets," *JFM*, 443, 2001, pp. 1-25.

[27]Greitzer, E. M., Tan, C. S., Graf, M. B., *Internal Flow: Concepts and Applications*, Cambridge U. Press, Cambridge Mass., 2004.

[28]Broadwell, J. E., Breidentahl, R. E., "Structure and Mixing of a Transverse Jet in Incompressible Flow," JFM, 148, 1984, pp. 405-412.

[29]Lamb, H, *Hydrodynamics*, 6th ed., Dover, Mineola, NY, 1932.

[30]Poroseva, S., Iaccarino, G., "Simulating Separated Flows Using the k-ε Model," Center for Turbulence Research TR, Annual Research Briefs, Stanford Univ., Stanford, CA, 2001, pp. 375–383, https://ctr. stanford.edu/annual-research-briefs-2001.

[31]Margarson, R. J., "Fifty Years of Jet in Crossflow Research," AGARD1-141, 1993

[32]Pratte, B. D., Baines, W. D., "Profiles of the Round Turbulent Jet in a Crossflow," J. *Hyd, Div. Proc. ASCE, Hyd*. 93, 1967, pp. 53-64.